Perspectives on Carbon Nanotubes and Graphene Raman Spectroscopy

Mildred S. Dresselhaus,*,†,‡ Ado Jorio,§ Mario Hofmann,† Gene Dresselhaus,|| and Riichiro Saito⊥

†Department of Electrical Engineering and Computer Science, Massachusetts Institute of Technology, Cambridge, Massachusetts 02139-4037, ‡Department of Physics, Massachusetts Institute of Technology, Cambridge, Massachusetts 02139-4037, §Department of Physics, UFMG, Belo Horizonte, MG 30123-970, Brazil, ||Francis Bitter Magnet Laboratory, Massachusetts Institute of Technology, Cambridge, Massachusetts 02139-4037, and ⊥Department of Physics, Tohoku University, Sendai, 980-8578, Japan

ABSTRACT Raman spectroscopy is here shown to provide a powerful tool to differentiate between two different sp² carbon nanostructures (carbon nanotubes and graphene) which have many properties in common and others that differ. Emphasis is given to the richness of both carbon nanostructures as prototype examples of nanostructured materials. A glimpse toward future developments in this field is presented.

KEYWORDS Graphene, carbon nanotubes, graphene ribbons, Raman spectroscopy

Carbon occurs in many forms, and the dependence of the properties of each form on its special structure makes carbon a truly unique building block for nanomaterials. For this reason carbon has been investigated for more than half a century without exhausting its wonders and challenges. Especially with the dawn of nanoscience now unfolding, we are still finding new properties for carbon nanostructures, thereby opening breathtaking opportunities for the discovery of new science and applications. We will here focus on one special form of carbon that has intrigued many scientists over the years, namely, sp² hybridized carbon.

> **Carbon has been investigated for more than half a century without exhausting its wonders and challenges.**

The ideal concept of sp² nanocarbons starts with a single monolayer graphene sheet denoted by 1-LG (see Figure 1a), the planar honeycomb lattice of sp² hybridized carbon atoms. Although this system can be large (ideally infinite in-plane), it is only one atom thick, thus representing a two-dimensional (2D) sp² nanocarbon containing two atoms per unit cell, A and B (Figure 1a). When two graphene sheets are stacked, what is called bilayer graphene (2-LG) is obtained (Figure 1b,c). Three sheets give three-layer graphene (3-LG), as shown in Figure 1d, and many graphene layers on top of each other yield graphite. A narrow strip of graphene (below 100 nm wide) is called a graphene nanoribbon, and a few of these nanoribbons can also be stacked to make a one-dimensional (1D) multilayer nanoribbon. In the formation of such multilayer nanoribbons, stacking order is important with the AB Bernal stacking, shown in Figure 1b−d, leading to the lowest energy geometry (ground state) and with an equilibrium c-axis lattice constant of 0.335 nm. Rolling-up a narrow strip of monolayer graphene in a seamless way into a cylinder forms what is called a single-wall carbon nanotube (SWNT, see Figure 1g). Conceptually, nanoribbons and nanotubes can be infinitely long, thus representing one-dimensional systems. By adding one- and two-layer concentric cylinders to a SWNT, we get double- and triple-wall carbon nanotubes, and by adding many rolled-up concentric cylinders, a multiwall carbon nanotube (MWNT) is obtained. A piece of graphite with small lateral dimensions (a few hundred nanometers and smaller) is called nanographite, which represents a zero-dimensional (0D) system.

Raman spectroscopy has historically played an important role in the study and characterization of graphitic materials,[1] being widely used over the last four decades to characterize pyrolytic graphite, carbon fibers,[1] glassy carbon, pitch-based graphitic foams,[2,3] nanographite ribbons,[4] fullerenes,[5] carbon nanotubes,[6,7,36] and graphene.[8] For sp² nanocarbons such as graphene and
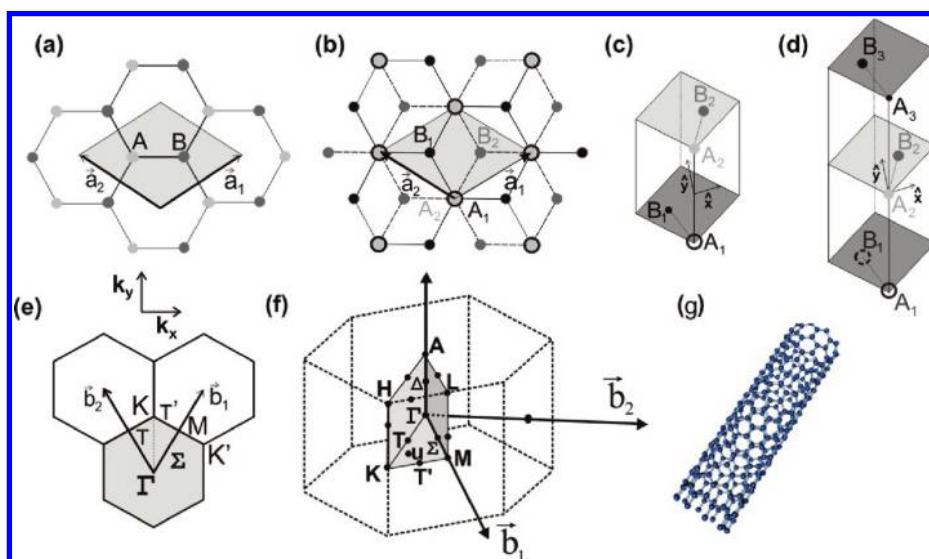
FIGURE 1. Schematics showing the structures of sp^2 nanocarbons. (a) Monolayer graphene (1-LG). The two vectors $\vec{a}_1$ and $\vec{a}_2$ define the unit cell (gray rhombus) containing two atoms A and B. (b) Bilayer graphene (2-LG). The unit vector, unit cell, and the four atoms (A$_1$, B$_1$ from one layer plus A$_2$, B$_2$ from the other) within the unit cell are displayed. (c) A three-dimensional (3D) view of (b). (d) A 3D view of the unit cell for three-layer graphene (3-LG). (e and f) The Brillouin zone for two-dimensional (2D) graphene and 3D graphite, respectively, showing the high symmetry points and lines, and the reciprocal space wavevectors $\vec{b}_1$ and $\vec{b}_2$. (g) A single-wall carbon nanotube (SWNT).[8]

carbon nanotubes, Raman spectroscopy can give information about crystallite size, clustering of the sp^2 phase, the presence of sp^2–sp^3 hybridization and the introduction of chemical impurities, the magnitude of the mass density, the optical energy gap, elastic constants, doping, defects and other crystal disorder, edge structure, strain, number of graphene layers, nanotube diameter, chirality, curvature, and finally the metallic vs semiconducting behavior and the science of excitons which make carbon nanotubes unique.[9] In this perspectives article, we consider three aspects of Raman spectra (see Figure 2), which are sensitive enough to provide unique information about the similarities and differences between the various carbon nanostructures. In this article, various Raman features are discussed including the G-band at ∼1582 cm^{-1}, which is common to all sp^2 carbon forms, the radial breathing mode (RBM) that makes the diameter and optical transition energy analysis of nanotubes possible, and the D and G′ bands that are significant in providing information about the electronic and geometrical structure through the double resonance process.[6−9,37] This discussion does not exhaust the richness of Raman spectra in sp^2 nanocarbons, which can exhibit many second- and higher-order modes, as well as new disorder-induced features (see Figure 2). The discussion given here does, however, provide a taste of the power of Raman spectroscopy.

The G-Band. The stretching of the C–C bond in graphitic materials gives rise to the so-called G-band Raman feature which is common to all sp^2 carbon systems (see Figures 2 and 3). This spectral feature is similar for graphenes and nanotubes but yet has properties capable of distinguishing one carbon nanostructure from another. When the bond lengths and angles of graphene are modi-
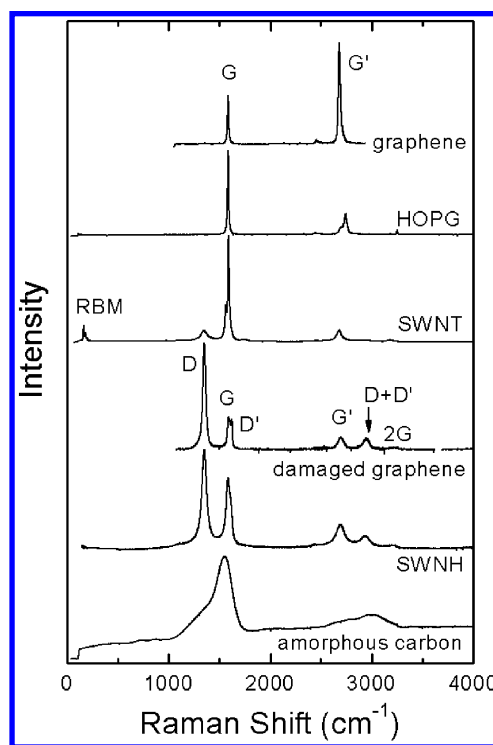

FIGURE 2. Raman spectra from different types of sp^2 nanocarbons. The graphene-related structures are labeled next to their respective spectra. The main features (RBM and disorder-induced D, D′ and D + D′ bands; first-order Raman-allowed G band; and second-order Raman overtones G′ (2iTO) and 2G) are labeled in some spectra, but the assignment applies to all of them. The detailed analysis of the frequency, line shape, and intensity for these features gives a great deal of information about each respective sp^2 carbon structure.

fied by strain, caused by the interaction with a substrate or with other graphene layers or due to external perturba-
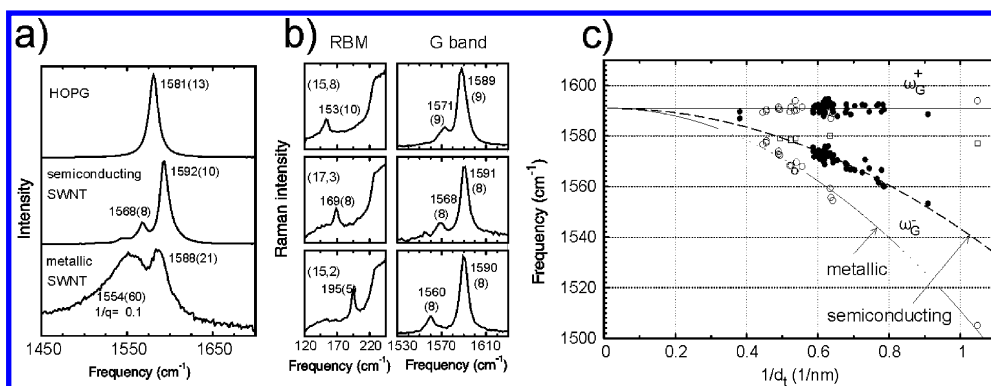
FIGURE 3. (a) The G-band for highly oriented pyrolytic graphite (HOPG), one semiconducting SWNT, and one metallic SWNT. (b) The RBM and the G-band Raman spectra for three semiconducting isolated SWNTs with the indicated (n,m) values. (c) Frequency vs $1/d_t$ for the two most intense G-band features (ω_{G^-} and ω_{G^+}) from isolated SWNTs. The lines are fits of the data, given by $\omega_G = 1591 - A/d_t^2$, where $A_{G^+} = 0$, $A_{G^-}{}^S = 47.7$ cm^{-1} nm^2, and $A_{G^-}{}^M = 79.5$ cm^{-1} nm^2 give the solid, dashed, and long dashed lines, respectively.[34]

tions, the hexagonal symmetry of graphene is broken.[8,10] The G-band is, therefore, highly sensitive to strain effects in sp^2 nanocarbons and can be used to probe any modification to the flat geometric structure of graphene, such as the strain induced by external forces, by one graphene layer on another in few layer graphene or in multiwall nanotubes, or even by the curvature of the side wall when growing a SWNT. Curvature effects, such as occur in carbon nanotubes, give rise to multiple peaks in the G-band spectrum for a SWNT,[6] while a single peak ($\omega_G \approx 1582$ cm^{-1}) is observed for a 2D graphene sheet (see Figure 3).[11,12] Up to six G-band phonons are Raman allowed in chiral SWNTs, although two of them (the totally symmetric A_1 modes, see Figure 3) usually dominate the spectra.[11,12] This curvature dependence generates a diameter dependence, thus making the G band a probe also for the tube diameter, while the G-band dependence on externally induced strain is very rich and is still controversial.[13]

The coupling between electrons and phonons in nanocarbons[14,15] has turned out to be especially interesting because of the breakdown of the adiabatic approximation, thus changing both the electron energies (the Peierls instability) and the phonon energies (Kohn anomaly effect) in somewhat different ways, thereby providing tools for studying differences in the properties of different carbon nanostructures. Since these effects are strongly dependent on the Fermi level and temperature, the G band becomes a probe for the doping of nanocarbons, thereby allowing study of their electronic dispersion relations. The Kohn anomaly is observed in metallic and semimetallic systems, where real electron–hole pair creation can occur by a phonon excitation ($\hbar\omega_G$) process, thus strongly influencing the G-band frequency and the spectral width of graphene and metallic SWNTs (see Figure 4). These effects in metallic SWNTs are stronger than those in graphene because of the quantum confinement effect, and this process depends sensitively on diameter and chiral angle.[38] In graphenes these effects depend sen-

sitively on the number of graphene layers. Semiconducting SWNTs also exhibit a phonon energy renormalization due to electron–phonon coupling, but this renormalization effect is weaker than that in graphene and for metallic SWNTs, and furthermore no real anomaly associated with ($E_g > \hbar\omega_G$) takes place for S-SWNTs. Consequently, while the G band line width in graphene and metallic SWNTs is strongly sensitive to whether or not the Fermi energy matches the energy of the Kohn anomaly,[38] in semiconducting SWNTs the G band line width is basically independent of doping.

The Radial Breathing Mode (RBM). The radial breathing mode is especially important in two ways: (1) for the determination of the diameter of a nanotube through the dependence of ω_{RBM} on d_t, and (2) for relating the ω_{RBM} and the resonant optical transition energies E_{ii} for a given tube. The status of research on these topics is summarized below.

Experimental data on the radial breathing mode frequency taken by many authors have been fit using the relation $\omega_{RBM} = A/d_t + B$. For the water-assisted supergrowth samples, values of $A = (227.0 \pm 0.3)$ nm·cm^{-1} and $B = (0.3 \pm 0.2)$ cm^{-1} are obtained. This result is in remarkably good agreement with elasticity theory[16] parametrized by the graphite elastic properties, thus directly connecting one-dimensional carbon nanotubes and their two-dimensional counterpart graphene from which nanotubes are conceptually derived. The vanishing value of B is in accordance with the limit $d_t \rightarrow \infty$ appropriate for a graphene sheet.

However, all the other ω_{RBM} results in the literature are upshifted from these values of A and B, due to the van der Waals interaction with the environment, and can be generally described by

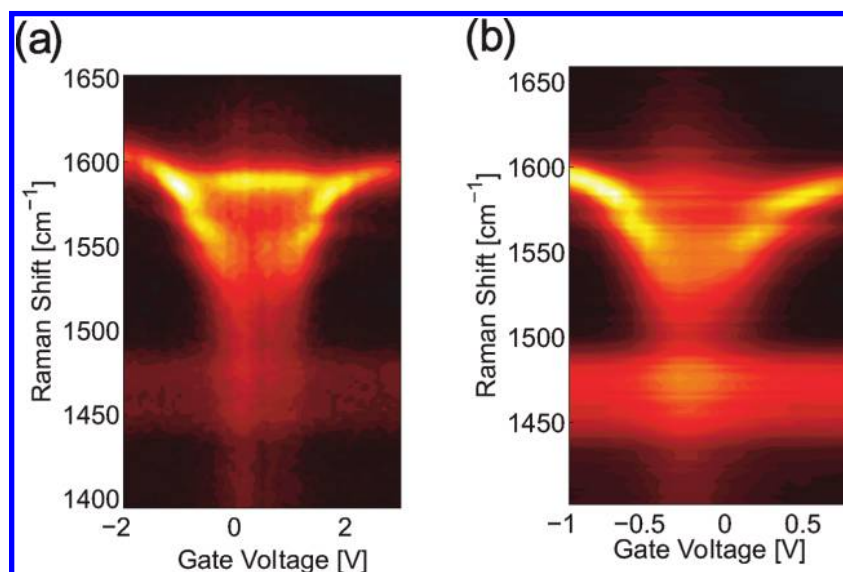$$\omega_{RBM} = \frac{227}{d_t}\sqrt{1 + C_e d_t^2} \qquad (1)$$

FIGURE 4. Experimental results for the Raman G band intensity as a function of applied gate voltage for two metallic SWNTs (a) and (b), showing variations in behavior due to differences in their chiralities. A strong (weak) intensity peak is denoted by the yellow (black) color.[35]

where the parameter C_e in eq 1 describes environmental effects.[16] The C_e values fitting the RBM results for several samples in the literature range from 0.05 (HiPCO@SDS, data from ref 17) to 0.07 (free-standing, data from ref 18). It is intriguing that the supergrowth sample is the only sample showing the pristine-like behavior, while the measured free-standing tubes show the highest level of environmental changes. However, the detailed science behind the specific values of C_e has not yet been adequately addressed.

The RBM also has been important for understanding the effect of tube−tube interaction within multiwall carbon nanotubes, the prototype material for studying such interactions being double-wall carbon nanotubes (DWNTs).[19] Since most spectroscopic experiments on DWNTs have been performed on bundles or solution-based samples, it has been inherently difficult to use such Raman spectra to investigate which inner (n,m) tubes are actually contained inside the variety of outer (n',m') tubes that have been observed in bundled samples. To address this difficulty, an investigation of the Raman spectra of 11 individual isolated peapod-derived DWNTs, all with (6,5) semiconducting inner tubes and all with the S@M inner/outer tube configuration, was performed using a single laser excitation energy of $E_{laser} = 2.10$ eV.[20] The outer tubes of the 11 DWNTs that are formed with a (6,5) inner tube can have different (n,m) designations from one another, but some will have common (n,m) chiralities. A plot of the RBM frequencies $\omega_{RBM,o}$ for the outer tube for such a DWNT as a function of $\omega_{RBM,i}$ for the inner tube showed that for these 11 individual isolated DWNTs, the RBM frequency $\omega_{RBM,o}$ for the outer tubes varies over a 12 cm^{-1} range, while $\omega_{RBM,i}$ for the inner tubes also does

not have a constant value, but rather varies over a range of 18 cm^{-1}. This 18 cm^{-1} variation in the RBM frequency $\omega_{RBM,i}$ for the inner tube is large, considering that all these inner tubes are (6,5) tubes. These experiments show us that in forming a DWNT, the inner and outer tubes impose considerable stress on one another, and this stress modifies their ω_{RBM} values very significantly, making the (n,m) identifcation of the inner and outer tubes of DWNTs much more complex than for SWNTs.

Finally, through the RBM resonance window analysis, we can also study the (n,m) dependence of the optical transition energies (E_{ii}). This analysis reveals a great deal of information that goes beyond the simple tight binding model, including $\sigma−\pi$ hybridization and the science of excitons. Though some aspects of the experiments can be interpreted within the context of a simple, noninteracting electron model,[21,22] it has become increasingly clear that electron−electron interactions also play an important role in determining the optical transition energies.

Figure 5a shows a 2D RBM map for the water-assisted chemical vapor deposition grown ("supergrowth", SG) SWNT sample.[25] This sample has a very broad diameter distribution and can therefore be used to gain a deep understanding of the SWNT optical properties. Figure 5b is a plot of all E_{ii}^{SG} obtained experimentally by fitting the resonance windows extracted from the data in Figure 5b, as a function of ω_{RBM}^{SG}. The observed E_{ii}^{SG} values range from E_{11}^{S} up to E_{66}^{S} and including E_{11}^{M} and E_{22}^{M} (the superscripts S stand for S-SWNTs and M for M-SWNTs). All the E_{ii}^{SG} data in Figure 5b can be fitted using an empirical equation that is given by[23−25]

$$E_{ii}(p,d_t) = \alpha_p \frac{p}{d_t}\left[1 + 0.467 \log\frac{0.812}{p/d_t}\right] + \beta_p \cos 3\theta/d_t^2$$

(2)

where p is defined as 1, 2, 3, ..., 8 for E_{11}^S, E_{22}^S, E_{11}^M, E_{33}^S, E_{44}^S, E_{22}^M, E_{55}^S, E_{66}^S, thus measuring the distance of the cutting line from the K point in the zone folding procedure. The fitting gives values $\alpha_p = 1.074$ for $p = 1, 2, 3$ and $\alpha_p = 1.133$ for $p \geq 4$. The β_p values in eq 2 for the lower (upper) E_{ii} branches are −0.07 (0.09), −0.18 (0.14), −0.19 (0.29), −0.33 (0.49), −0.43 (0.59), −0.6 (0.57), −0.6 (0.73), and −0.65 (unknown) for $p = 1, 2, 3, ..., 8$, respectively.[24,25] The functional form in eq 2 carries a linear dependence of E_{ii} on p/d_t, expected from tight binding theory plus quantum confinement of the 2D electronic structure of graphene, a logarithmic correction term that comes from many-body interactions, and a θ dependent term which includes electronic trigonal warping and chirality-dependent curvature effects ($\sigma-\pi$ hybridization).[23] While the empirical eq 2 is useful for easily building a Kataura plot as in Figure 5, the full theoretical understanding of E_{ii} vs (n,m) requires the development of an extended tight binding calculation, including both excitonic effects, through solution of the Bethe−Salpeter equation,[28] and dielectric screening from σ and core electrons, as well as from the SWNT environment. Efforts are now being made to accurately determine the (n,m) dependence for the RBM Raman cross section, so that such RBM experiments can be used for an (n,m) population

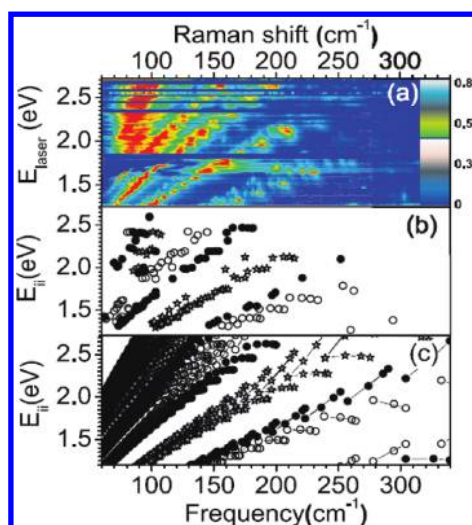FIGURE 6. The G′ spectra for graphene as a function of the number of layers.[8]

FIGURE 5. (a) RBM resonance Raman map for the "supergrowth" (SG) SWNT sample. The scale on the right indicates the relative intensities of experimental data. (b) Kataura plot of all transition energies (E_{ii}^{SG}) that could be experimentally obtained from the resonance windows extracted from (a), as a function of ω_{RBM}. (c) The Kataura plot obtained from eq 2 with the parameters that best fit the data in (b). The stars stand for M-SWNTs, the open bullets stand for type I S-SWNTs, and the filled bullets stand for type II S-SWNTs, where type I and type II refer to whether the modulus or remainder of $(2(n + m),3)$ is 1 or 2, respectively, for these S-SWNTs.[25]
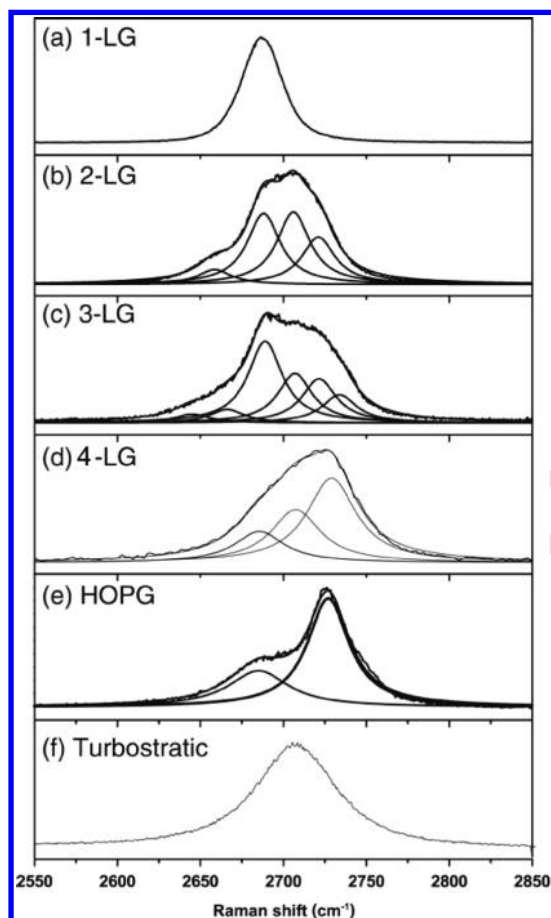
analysis and to more deeply understand environmental screening in 1D systems.

Dispersive G′-Band: the Double Resonance Process. All kinds of sp^2 carbon materials exhibit a strong Raman feature which appears in the range 2500−2800 cm^{-1}, as shown in Figure 2. Together with the G band (1582 cm^{-1}), this spectrum is a Raman signature of graphitic sp^2 materials and is called the G′ band to emphasize that it is a Raman-allowed mode for sp^2 carbons. Interestingly, the G′ band is a second-order two-phonon process and, intriguingly, it exhibits a strong frequency dependence on the excitation laser energy E_{laser}. This *dispersive behavior* ($\omega_{G'} = \omega_{G'}(E_{laser})$) is unusual in Raman scattering, since Raman-active mode frequencies usually do not depend on E_{laser}. The G′ band in particular is a second-order process related to a phonon near the K point in graphene, activated by double resonance (DR) processes,[27,28] which are responsible for its dispersive nature and cause a strong dependence on any perturbation to the electronic and/or phonon structure of graphene. For this reason, the G′ feature provides a very sensitive probe for characterizing specific sp^2 nanocarbons. For example, the G′ band can be used for differentiating between single and double-
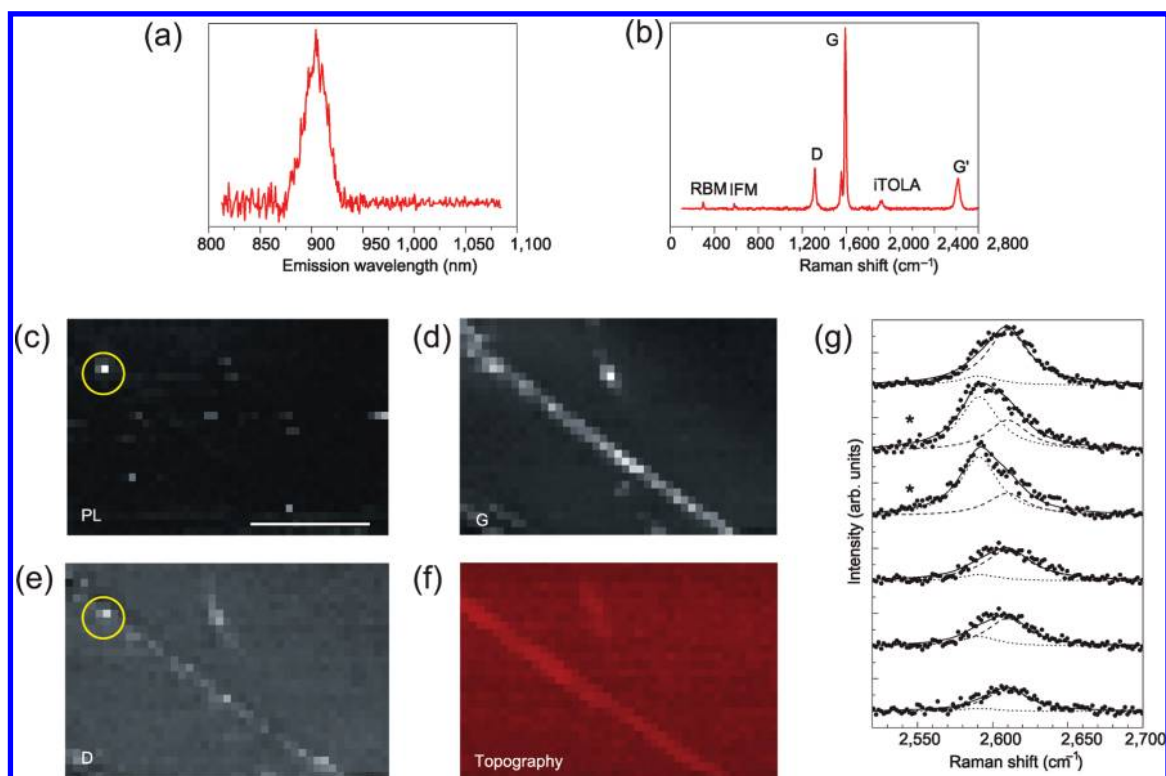
FIGURE 7. Localized excitonic emission in a semiconducting SWNT observed by near field spectroscopy. (a) Photoluminescence emission at $\lambda = 900$ nm. (b) Raman spectrum recorded from the same SWNT. (c) Near-field photoluminescence image of the same SWNT revealing localized excitonic emission. (d−e) Near-field Raman imaging of the same SWNT, where the image contrast is provided by spectral integration over the G- and D-bands, respectively. (f) Corresponding topography image. The yellow circles indicate localized photoluminescence (c) and defect-induced (D band) Raman scattering (e). The scale bar in (c) denotes 250 nm, which applies to the entire figure.[29] (g) G′-band spectra taken at different locations along a single individual SWNT. The two spectra indicated by * were measured at the defect locations indicated in (c,e).[29]

layer graphene with AB interlayer stacking[8] and for probing aspects of the electronic structures of SWNTs.

Figure 6 shows the dependence of the G′ band on the number of layers.[8] While 1-LG exhibits a single very intense Lorentzian peak, fitting the 2-LG G′-band requires four Lorentzians, which are related to the four possible double resonance scattering processes, rather than to one possible process for 1-LG, resulting from the splitting of the π electronic structure of graphene when a second layer is added. With an increase in the number of layers, the number of DR scattering processes increases, and eventually the line shape converges to graphite, where only two peaks are observed.[8]

Finally, carbon nanotubes show a very special G′ feature, where the number of peaks and their frequencies depend on (n,m) due to both curvature-induced strain and quantum confinement effects.[6] Recently it was shown that the G′ feature can be used to assign p- and n-type doping in SWNTs, where the spectra from one single dopant attached to an individual tube was observed using both near-field Raman microscopy and spectroscopy,[29] as shown in Figure 7. Near-field spectroscopy can drive the spacial resolution down to ∼10 nm, thus making it possible to probe local effects. Figure 7 shows localized pho-

toluminescence emission (see Figure 7a,c), and at the same physical location, changes in the G′-band are observed (see Figure 7g and details in ref 29) along with the observation of a strong disorder-induced (D band) feature (see Figure 7b,e), as discussed in the next section.

Disorder-Induced D Band. The presence of disorder in sp^2-hybridized carbon systems leads to rich and intriguing phenomena in their resonance Raman spectra, thus making Raman spectroscopy one of the most sensitive and informative techniques to characterize disorder in sp^2 carbon materials. Raman spectroscopy has thus become a key tool and is widely used to identify disorder in the sp^2 network of different carbon structures, such as diamond-like carbon, amorphous carbon, nanostructured carbon, as well as carbon nanofibers, nanotubes, and nanohorns.[9,30−32]

Figure 8a shows the Raman spectra of crystalline graphene, exhibiting the first-order Raman-allowed G-band, before ion implantation is used to introduce defects into graphene systematically and in a controlled manner. When graphene is bombarded by a low ion dose (10^{11} Ar^+/cm^2), point defects are formed and the Raman spectra of the disordered graphene exhibit two new sharp features appearing at 1345 and 1626 cm^{-1} for $E_{laser} = 2.41$
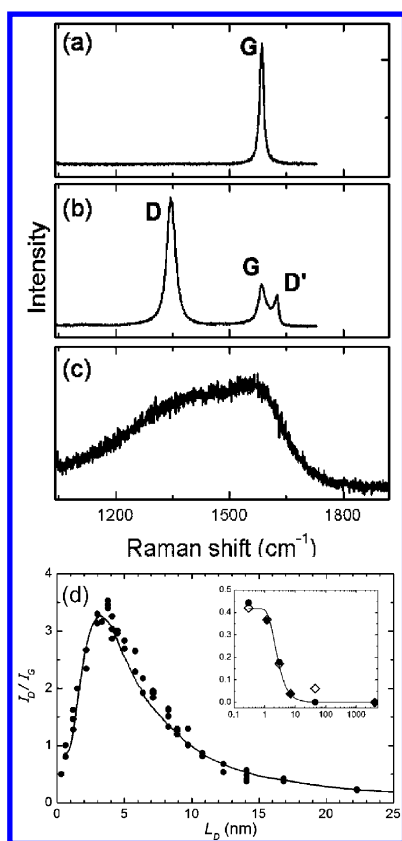
FIGURE 8. The first-order Raman spectrum of (a) crystalline graphene, (b) defective graphene, and (c) and fully disordered single-layer graphene deposited on a SiO₂ substrate. These spectra are all obtained with $E_{laser} = 2.41$ eV. (d) The I_D/I_G data points from three different monolayer graphene samples as a function of the average distance L_D between defects, induced by the ion bombardment procedure. The solid line is the result of a modeling calculation. The inset to (d) shows I_D/I_G vs L_D plotted on a log scale for the L_D axis for two ion-implanted graphite samples.[32] The different behaviors being due to the presence of under layers untouched by the ion beam.

eV, as seen in Figure 8b.[32] These two features have, respectively, been called D- and D′-bands, to denote disorder. These bands are dispersive, and they are observed at these special frequencies when excited with a 514 nm wavelength (2.41 eV) laser. Finally, when the periodic system is strongly disordered by a large ion dose (10^{15} Ar⁺/cm²), the Raman spectrum resembles the profile of the density of states for the higher-energy optical phonon branch (Figure 8c).

Quantifying disorder in a graphene monolayer is usually made by analyzing the I_D/I_G intensity ratio between the disorder-induced D-band and the Raman allowed G-band. Consecutive Ar⁺ ion bombardment and Raman spectroscopy experiments were performed on monolayer graphene samples. The evolution of the resulting I_D/I_G data as a function of the average distance between defects L_D is shown in Figure 8d. Here we see that the I_D/I_G ratio has a nonmonotonic dependence on L_D, increasing with increasing L_D up to $L_D \sim 4$ nm where I_D/I_G has a peak value, and then decreasing for $L_D > 4$ nm. Such behavior has

been explained by the existence of two disorder-induced competing mechanisms contributing to the Raman D-band. These competing mechanisms are the basis for a phenomenological model for the L_D dependence of I_D/I_G, as described by Lucchese et al.[32]

> Besides defect quantification, it is important to discuss how disorder depends on the specific defect.

An example of a result that was successful in distinguishing different defects from one another is the study of the edge of a graphite sample, analyzing the orientation of the carbon hexagons to determine the crystallographic orientation of these edges. In this way the so-called zigzag edge arrangements were distinguished from the armchair or random atomic edge structures.[4] The armchair (zigzag) structure can be identified spectroscopically by the presence (absence) of the D-band. This effect can be understood by applying double resonance theory to a semi-infinite graphite crystal and by considering the one-dimensional character of the defect, as discussed in ref 4. More effort has now to be devoted to finding the specific signatures of specific structural disorder in graphene systems.

Summary and Perspectives. Throughout the nearly one century of Raman spectroscopy that has been used to study the science of sp² carbon materials, more and more fundamental aspects of their electronic and vibrational properties have been revealed. This nonstop development is due to improvements in both experimental techniques and theoretical calculations and due to advances in nanosciences generally. From the experimental side, near-field optics can now unravel Raman spectra with spacial resolution below the diffraction limit, a former limitation for Raman spectroscopy. Time-dependent Raman and coherent-phonon spectroscopy[33,34] provide new frontiers for vibrational spectroscopy, although this topic was not discussed here. From the theoretical side, the simplicity of sp² carbon materials (containing only one atom species on a hexagonal structure) made possible the development of fancy tight binding and first-principles calculations reaching unprecedented levels of accuracy for the description of electronic and vibrational levels, where new theoretical insights, such as electron−electron correlation, excitonic effects, and electron−phonon interactions, were successfully applied to sp² nanocarbons but now can perhaps be applied to other systems. Measuring the Raman signal from one single-layer sheet of atoms, or from one

single rolled up nanotube, together with the ability to apply controlled perturbations to these nanomaterials (strain, doping, etc.) has achieved an unprecedented level of detail in describing the physics of sp^2 carbons but has at the same time also raised more fundamental questions. The experience gained from these studies indicates that Raman spectroscopy and carbon nanostructures remain active vehicles for the discovery of new physics.

REFERENCES AND NOTES

(1) Dresselhaus, M. S.; Dresselhaus, G.; Sugihara, K.; Spain, I. L.; Goldberg, H. A. *Graphite Fibers and Filaments*; Springer-Verlag: Berlin, 1988; Vol. 5.

(2) Klett, J.; Hardy, R.; Romine, E.; Walls, C.; Burchell, T. *Carbon* **2000**, *38* (7), 953–973.

(3) Barros, E. B.; Demir, N. S.; Souza, A. G.; Mendes, J.; Jorio, A.; Dresselhaus, G.; Dresselhaus, M. S. *Phys. Rev. B* **2005**, *71* (16), 165422.

(4) Cancado, L. G.; Pimenta, M. A.; Neves, B. R. A.; Medeiros-Ribeiro, G.; Enoki, T.; Kobayashi, Y.; Takai, K.; Fukui, K.; Dresselhaus, M. S.; Saito, R.; Jorio, A. *Phys. Rev. Lett.* **2004**, *93* (4), 047403.

(5) Dresselhaus, M. S.; Dresselhaus, G. *Science of Fullerenes and Carbon Nanotubes*. Academic Press: San Diego, CA, 1996.

(6) Dresselhaus, M. S.; Dresselhaus, G.; Saito, R.; Jorio, A. *Phys. Rep.* **2005**, *409* (2), 47–99.

(7) Saito, R.; Dresselhaus, G.; Dresselhaus, M. S. *Physical Properties of Carbon Nanotubes*. Imperial College Press: London, 1998.

(8) Malard, L. M.; Pimenta, M. A.; Dresselhaus, G.; Dresselhaus, M. S. *Phys. Rep.* **2009**, *473* (5–6), 51–87.

(9) Ferrari, A. C.; Robertson, J. *Philos. Trans. R. Soc. London, Ser. A* **2004**, *362* (1824), 2477–2512.

(10) Ni, Z. H.; Yu, T.; Lu, Y. H.; Wang, Y. Y.; Feng, Y. P.; Shen, Z. X. *ACS Nano* **2008**, *2* (11), 2301–2305.

(11) Dresselhaus, M. S.; Eklund, P. C. *Adv. Phys.* **2000**, *49* (6), 705–814.

(12) Dresselhaus, M. S.; Dresselhaus, G.; Jorio, A.; Souza, A. G.; Saito, R. *Carbon* **2002**, *40* (12), 2043–2061.

(13) Cronin, S. B.; Swan, A. K.; Unlu, M. S.; Goldberg, B. B.; Dresselhaus, M. S.; Tinkham, M. *Phys. Rev. Lett.* **2004**, *93* (16), 167401.

(14) Dubay, O.; Kresse, G.; Kuzmany, H. *Phys. Rev. Lett.* **2002**, *88* (23), 235506.

(15) Piscanec, S.; Lazzeri, M.; Mauri, F.; Ferrari, A. C.; Robertson, J. *Phys. Rev. Lett.* **2004**, *93* (18), 185503.

(16) Araujo, P. T.; Maciel, I. O.; Pesce, P. B. C.; Pimenta, M. A.; Doorn, S. K.; Qian, H.; Hartschuh, A.; Steiner, M.; Grigorian, L.; Hata, K.; Jorio, A. *Phys. Rev. B* **2008**, *77* (24), 241403.

(17) Bachilo, S. M.; Balzano, L.; Herrera, J. E.; Pompeo, F.; Resasco, D. E.; Weisman, R. B. *J. Am. Chem. Soc.* **2003**, *125* (37), 11186–11187.

(18) Paillet, M.; Michel, T.; Meyer, J. C.; Popov, V. N.; Henrard, L.; Roth, S.; Sauvajol, J. L. *Phys. Rev. Lett.* **2006**, *96* (25), 039704.

(19) Pfeiffer, R.; Pichler, T.; Kim, Y.; Kuzmany, H. Double-Wall Carbon Nanotubes. In *Carbon Nanotubes. Advanced Topics in the Synthesis, Structure, Properties and Applications*; Jorio, A., Dresselhaus, M., Dresselhaus, G., Eds.; Springer: Berlin/Heidelberg, 2008; pp 495–530.

(20) Villalpando-Paez, F.; Son, H.; Chou, S. G.; Samsonidze, Ge. G.; Kim, Y. A.; Muramatsu, H.; Hayashi, T.; Endo, M.; Terrones, M.; Dresselhaus, M. S. *Phys. Rev. B* **2009**, *80* (3), 035419-(1-14).

(21) Jorio, A.; Fantini, C.; Pimenta, M. A.; Capaz, R. B.; Samsonidze, G. G.; Dresselhaus, G.; Dresselhaus, M. S.; Jiang, J.; Kobayashi, N.; Gruneis, A.; Saito, R. *Phys. Rev. B* **2005**, *71* (7), 075401.

(22) Samsonidze, Ge. G.; Saito, R.; Kobayashi, N.; Gruneis, A.; Jiang, J.; Jorio, A.; Chou, S. G.; Dresselhaus, G.; Dresselhaus, M. S. *Appl. Phys. Lett.* **2004**, *85* (23), 5703–5705.

(23) Araujo, P. T.; Doorn, S. K.; Kilina, S.; Tretiak, S.; Einarsson, E.; Maruyama, S.; Chacham, H.; Pimenta, M. A.; Jorio, A. *Phys. Rev. Lett.* **2007**, *98* (6), 067401.

(24) Doorn, S. K.; Araujo, P. T.; Hata, K.; Jorio, A. *Phys. Rev. B* **2008**, *78* (16), 165408.

(25) Araujo, P. T.; Jorio, A. *Phys. Status Solidi B* **2008**, *245* (10), 2201–2204.

(26) Thomsen, C.; Reich, S. *Phys. Rev. Lett.* **2000**, *85* (24), 5214–5217.

(27) Saito, R. et al. *Phys, Rev, Lett.* **2001**, *88*, 027401.

(28) Jiang, J.; Saito, R.; Samsonidze, Ge. G.; Jorio, A.; Chou, S. G.; Dresselhaus, G.; Dresselhaus, M. S. *Phys. Rev. B* **2007**, *75* (3), 035407.

(29) Maciel, I. O.; Anderson, N.; Pimenta, M. A.; Hartschuh, A.; Qian, H. H.; Terrones, M.; Terrones, H.; Campos-Delgado, J.; Rao, A. M.; Novotny, L.; Jorio, A. *Nat. Mater.* **2008**, *7* (11), 878–883.

(30) Pimenta, M. A.; Dresselhaus, G.; Dresselhaus, M. S.; Cancado, L. G.; Jorio, A.; Saito, R. *Phys. Chem. Chem. Phys.* **2007**, *9* (11), 1276–1291.

(31) *Carbon Nanotubes. Advanced Topics in the Synthesis, Structure, Properties and Applications*; Jorio, A., Dresselhaus, M., Dresselhaus, G., Eds.; Springer: Berlin/Heidelberg, 2008; Vol. 111, pp 495–530.

(32) Lucchese, M. M.; Stavale, F.; Ferreira, E. H.; Vilane, C.; Moutinho, M. V. O.; Capaz, R. B.; Achete, C. A.; Jorio, A. *Carbon*, In press, doi: 10.1016/j.carbon.2009.12.057.

(33) Kato, K.; Ishioka, K.; Kitajima, M.; Tang, J.; Saito, R.; Petek, H. *Nano Lett.* **2008**, *8*, 3102–3108.

(34) Jorio, A.; Souza, A. G.; Dresselhaus, G.; Dresselhaus, M. S.; Swan, A. K.; Unlu, M. S.; Goldberg, B. B.; Pimenta, M. A.; Hafner, J. H.; Lieber, C. M.; Saito, R. *Phys. Rev. B* **2002**, *65* (15), 155412.

(35) Farhat, H.; Son, H.; Samsonidze, G. G.; Reich, S.; Dresselhaus, M. S.; Kong, J. *Phys. Rev. Lett.* **2007**, *99* (14), 145506.

(36) Jorio, A.; Pimenta, M. A.; Souza Filho, A. G.; Satio, R.; Dresselhaus, G.; Dresselhaus, M. S. *New J. Phys.* **2003**, *5*, 139.1–139.17.

(37) Satio, R.; Gruneis, A.; Samsonidze, Ge G.; Brar, V. W.; Dresselhaus, G.; Dresselhaus, M. S.; Jorio, A.; Cancado, L. G.; Fantini, C.; Pimenta, M. A.; Souza Filho, A. G. *New J. Phys.* **2003**, *5*, 157.1–157.15.

(38) Sasaki, K.; Saito, R.; Dresselhaus, G.; Dresselhaus, M. S.; Farhat, H.; Kong, J. *Phys. Rev. B* **2008**, *77*, 245441.

(39) Sanders, G. D.; Stanton, C. J.; Kim, J.-H.; Yee, K.-J.; Lim, Y.-S.; Haroz, E. H.; Booshehri, L. G.; Kono, J.; Saito, R. *Phys. Rev. B* **2009**, *79*, 205434-1-19.